MIXED ELEMENT FORMULATION FOR THE FINITE ELEMENT-BOUNDARY INTEGRAL METHOD

J. Meese[1], L.C. Kempel[2], and S.W. Schneider[3]
[1]General Dynamics Advanced Information Systems, Ypsilanti, MI 48197
[2]Michigan State University, East Lansing, MI 48824-1226
[3]Air Force Research Laboratory, Sensors Directorate, Wright-Patterson AFB, OH 45433

Abstract – A mixed element approach using right hexahedral elements and right prism elements for the finite element-boundary integral method is presented and discussed for the study of planar cavity-backed antennas. The mixed element method is shown to decrease the required computation time for geometrically constrained geometries by reducing the unknown count on the open aperture on the cavity. By reducing the unknown count on the surface, the memory and computational cost associated with the boundary integral portion of the solution is decreased versus solutions using only prism elements. The accuracy of the mixed element approach is shown to be comparable with that of a single element approach, especially for far field parameters such as radiation pattern and radar cross section.

I. INTRODUCTION

Efficient numerical modeling of antennas is an integral part of the antenna design process. Numerical modeling can aid in the rapid design of an antenna prior to prototype fabrication, therefore drastically reducing the design time and reducing cost. One of the challenges inherent in the numerical modeling of antennas is how to model the antenna in the most accurate, yet efficient manner.

Various numerical techniques have been used to model antennas with size on the order of a few wavelengths. One of the most popular of these techniques is formulated using an integral equation (IE) and implemented using the Method of Moments (MoM) or one of its variants. One particularly relevant example, a spiral antenna, is given in [0]. While this method is highly accurate and well studied, it suffers from the fact that it produces fully dense matrices leading to memory demands of $O(N^2)$ and computational complexity of $O(N^3)$ where N is the order of system. In addition, the most efficient MoM formulations are based on surface equivalence and hence are restricted to piecewise homogeneous materials.

Recently, techniques have been developed to reduce the computational complexity of integral equation formulations to $O(N \log_2 N)$ by exploiting the fact that many of the unknowns are physically distant from other unknowns [0]. A different approach, the Finite Element (FE) method [0-0], is based on a partial differential equation (PDE) approach and therefore leads to very sparse system matrices that can be stored and solved in a very efficient manner. In addition, since it is a PDE-based approach, the FE method readily permits analysis of inhomogeneous materials in an antenna design. However, the FE method does not enforce the Sommerfeld radiation condition for electromagnetic waves as part of its formulation and hence is susceptible to spurious reflections from the mesh truncation surface. To solve this problem, often local conditions, such as an absorbing boundary condition (ABC) or

Perfectly Matched Layers (PML) are used. These methods are particularly useful for scattering calculations since the Radar Cross Section (RCS) is a far-zone quantity and hence the effect of local errors on the solution tends to be diminished via integration. Solution accuracy is a particular concern for antenna modeling using such an approximate condition since important antenna parameters (e.g. input impedance, mutual impedance, etc.) depend on accurate local field solutions. A technique combining the FE method and an integral equation, termed the Finite Element-Boundary Integral (FE-BI) method, is an attractive alternative since it implements an exact relationship between tangential electric and magnetic fields on the mesh boundary as well as the Sommerfeld radiation condition [0-0] via a properly constructed Green's function. A third approach uses a harmonic expansion of the exterior field as a mesh closure condition [0]. An excellent summary of these various conditions is given in [0].

However, the FE-BI method suffers from a well-known drawback: The boundary integral portion of the system takes up the majority of memory and time for solution. In two dimensional cases, the use of triangular elements on the surface of the geometry to achieve the greatest modeling flexibility can lead to electrical oversampling which causes larger than needed memory demand and computational time. Quadrilateral elements, while not as flexible in modeling, can be used to reduce the unknown count for some cases [0], e.g. narrow slots. The mixture of triangular and quadrilateral elements can therefore allow a flexible modeling solution while reducing the effects of oversampling. For the case of three-dimensional cavity-backed antennas, quadrilateral elements can be extruded into right hexahedral elements while triangular elements can be extruded into right prism elements. Hence, the volumetric efficiency of quadrilateral elements can be combined with the flexibility of prisms to reduce overall complexity of a solution.

This paper presents the mixed element formulation as applied to three-dimensional cavity-backed antennas. Section II of the paper develops the theory for the mixed element formulation. Section III shows some numerical results comparing the mixed element formulation with the single element formulation. Section IV compares the computational time required for the two methods. Section V presents some conclusions and future directions for this work.

II. FORMULATION

Figure 1 illustrates a cavity-backed aperture lying in an infinite, metallic groundplane. The computational, and antenna, volume is denoted by V while the aperture is denoted by S. The portion of the groundplane, including any metal in the aperture, is indicated by S_{pec}. The fields within the computational volume are denoted by $(\mathbf{E}^{int}, \mathbf{H}^{int})$ while the external fields are indicated by $(\mathbf{E}^{ext}, \mathbf{H}^{ext})$. The material within the cavity may in general be inhomogeneous and anisotropic; however, for this work a simplified formulation assuming isotropic materials is presented. Expressions for anisotropic cases can be found for prisms in [0] while expressions for hexahedral elements may be similarly developed.

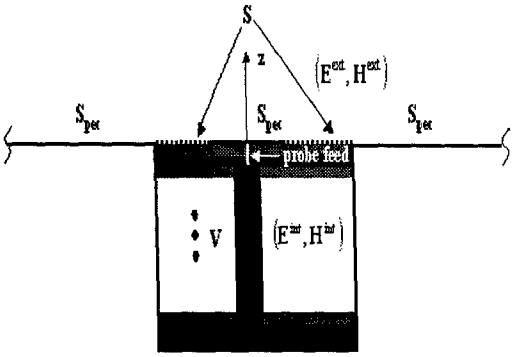

Figure 1: Cavity backed aperture recessed in an infinite ground plane with multiple loading layers.

This type of geometry represents flush-mounted cavity-backed antennas where the local surface in the vicinity of the antenna is planar. Antennas found in this type of configuration include both narrow bandwidth apertures (e.g. microstrip and slot antennas) as well as wide bandwidth apertures (e.g. packed elements such as I-dipoles as well as spiral and log-periodic antennas). A systematic modeling of these antennas through the use of highly efficient computational algorithms is important to determine the optimal configuration of these systems.

The problem domain is separated into two distinct regions, the region composed of the interior volume of the geometry, and the region composed of the surrounding free space area above the ground plane. The interior, FE, region is then coupled to the exterior, BI, region by enforcing tangential magnetic field continuity, $\hat{n}\times\mathbf{H}^{ext}=\hat{n}\times\mathbf{H}^{int}$, on the aperture surface (S) while tangential electric field continuity, $\hat{n}\times\mathbf{E}^{ext}=\hat{n}\times\mathbf{E}^{int}$, on that same surface is assured via the use of similar basis function for the interior and exterior representations. The final hybrid expression, usually known as the finite element-boundary integral equation, is given by

$$\frac{1}{\mu_r}\int_{V_i}(\nabla\times\mathbf{L}_i)\cdot(\nabla\times\mathbf{E}^{int})\,dV-k_0^2\varepsilon_r\int_{V_i}\mathbf{L}_i\cdot\mathbf{E}^{int}\,dV-$$
$$k_0^2\int_{S_i}\int_{S_j}\mathbf{L}_i\cdot\left(\hat{z}\times\bar{\bar{G}}_{e2}(x,y|x',y')\times\hat{z}\right)\cdot\mathbf{E}^{int}\,dS'\,dS=$$
$$-jk_0Z_0\int_{V_i}\mathbf{L}_i\cdot\mathbf{J}^{imp}\,dV \qquad (1)$$

where $\mathbf{L}_i$ is the vector testing function associated with the i^{th} row while $\mathbf{J}^{imp}$ represents an impressed current source as the antenna feed. The relative material parameters, ε_r and μ_r, are associated with each element and may vary on an element-by-element basis while k_0 and Z_0 are the free-space wavenumber and wave impedance, respectively. The electric dyadic Green's function of the second kind, $\bar{\bar{G}}_{e2}$, is taken to be the half-space Green's function [0].

The unknown electric field is expanded using the same functions as used for testing (e.g. Galerkin's method) is

$$\mathbf{E}^{int}=\sum_{j=1}^{N}E_j\mathbf{L}_j \qquad (2)$$

where E_j indicates complex-valued unknown expansion coefficients. Inserting (2) into (1), the final expression is given as

$$\sum_{j=1}^{N}E_j\left\{\begin{array}{l}\frac{1}{\mu_r}\int_{V_i}(\nabla\times\mathbf{L}_i)\cdot(\nabla\times\mathbf{L}_j)\,dV-k_0^2\varepsilon_r\int_{V_i}\mathbf{L}_i\cdot\mathbf{L}_j\,dV\\ -k_0^2\int_{S_i}\int_{S_j}\mathbf{L}_i\cdot\left(\hat{z}\times\bar{\bar{G}}_{e2}(x,y|x',y')\times\hat{z}\right)\cdot\mathbf{L}_j\,dS'dS\end{array}\right\}=$$
$$-jk_0Z_0\int_{V_i}\mathbf{L}_i\cdot\mathbf{J}^{imp}dV. \qquad (3)$$

This matrix equation is separated into two parts, one representing the finite element portion, written as I_{ij}^{FE}, and the other representing the boundary integral portion, written as I_{ij}^{BI} as

$$I_{ij}^{FE}=\frac{1}{\mu_r}\int_{V_i}(\nabla\times\mathbf{L}_i)\cdot(\nabla\times\mathbf{L}_j)\,dV$$
$$-k_0^2\varepsilon_r\int_{V_i}\mathbf{L}_i\cdot\mathbf{L}_j\,dV\,, \qquad (4)$$

$$I_{ij}^{BI}=$$
$$-k_0^2\int_{S_i}\int_{S_j}\mathbf{L}_i\cdot\left(\hat{z}\times\bar{\bar{G}}_{e2}(x,y|x',y')\times\hat{z}\right)\cdot\mathbf{L}_j\,dS'dS \qquad (5)$$

where the latter has support only when both test and source edges lie in the aperture. These integrals represent the matrix entries in the following linear system

$$\begin{bmatrix}I_{ij}^{FE}+I_{ij}^{BI} & I_{ij}^{FE}\\ I_{ij}^{FE} & I_{ij}^{FE}\end{bmatrix}\begin{Bmatrix}E_j^{S}\\ E_j^{int}\end{Bmatrix}=\begin{Bmatrix}0\\ f_i^{int}\end{Bmatrix} \qquad (6)$$

where E_j^S indicates unknown field expansion coefficients associates with the aperture surface, E_j^{int} are the expansion coefficients for the interior basis vectors and f_i^{int} is the excitation term associated with an interior

current source. Evaluation of (4) and (5) require specification of the basis functions, $\mathbf{L}_j$. These will be different for the different types of elements used in the mesh; hence their will be two different specifications of I_{ij}^{FE}, one for prisms and one for hexahedra, and four different specifications of I_{ij}^{BI} to represent all possible combinations of surface element coupling. The functions for a right prism are presented first followed by those for a right hexahedral.

Right Prisms

Right prism elements have been used successfully in the FE-BI method in the past [0]. These basis functions posses the required properties to be used in the FE-BI method. They enforce tangential field continuity across element faces and are curl conforming. The elements used in this work are also divergence-free and CT/LN elements [0].

Prisms have the advantage of providing great flexibility in modeling geometries that are irregular in two dimensions but regular in the third dimension, such as cavities recessed in ground planes, the case presented here. Prisms also have the advantage of making it quite simple to extrude a three-dimensional mesh from a two-dimensional mesh composed of triangles. In addition, the prism basis functions are derived from the two dimensional basis functions for triangles so they reduce to the two-dimensional triangular basis functions used in the boundary integral; hence, prisms are similar to triangle elements and therefore automatically enforce the essential boundary condition in the aperture. However, for some geometries such as narrow slot spiral antennas, prism elements have the disadvantage of oversampling the aperture and therefore inefficiently using resources. Figure 2 illustrates one possible realization of a right prism element where the local node numbering scheme is shown along with the encircled local edge numbering scheme.

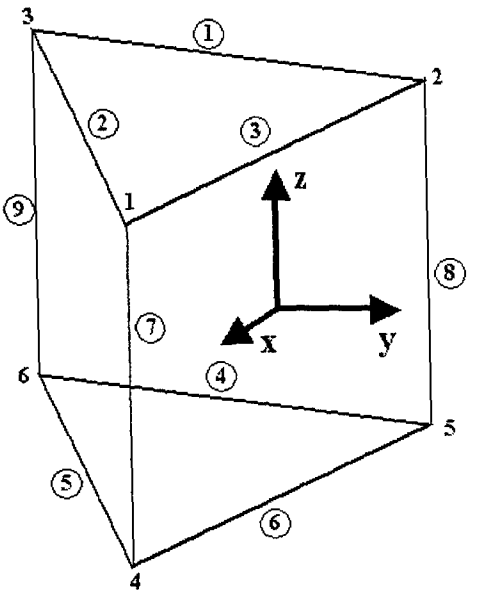

Figure 2: Right prism element shown with its defined local nodes and local edges (encircled numbers).

The nodes are ordered in a counter-clockwise direction in order to ensure that the normal vector of the element points towards the top of the element and therefore points out of the computational volume in the aperture of a cavity-backed antenna. The edge-based expansion functions for the prism element are derived from the Rao-Wilton-Glisson (RWG) basis functions for triangles [0] with a linear depth variation to allow for three-dimensional support. Assigning prism vector expansion functions as $\mathbf{L}_i = \mathbf{W}_i$, the nine vector functions associated with the prism are given by

$$\mathbf{W}_{\chi i} = \mathbf{V}_i = \frac{(z-z_i)}{c}\frac{l_i s_i}{2S^e}\left[(x-x_i)\hat{\mathbf{y}} - (y-y_i)\hat{\mathbf{x}}\right], \quad \chi = 1,2,3,$$
$$\mathbf{W}_{\chi i} = \mathbf{M}_i = \frac{(z_i-z)}{c}\frac{l_i s_i}{2S^e}\left[(x-x_i)\hat{\mathbf{y}} - (y-y_i)\hat{\mathbf{x}}\right], \quad \chi = 4,5,6,$$
$$\mathbf{W}_{\chi i} = \mathbf{K}_i = \frac{\hat{\mathbf{z}}}{2S^e}\left[(x_{k1}y_{k2} - x_{k2}y_{k1}) + (y_{k1} - y_{k2})x + (x_{k2} - x_{k1})y\right], \quad \chi = 7,8,9, \tag{7}$$

where l_i is the length of the i^{th} edge, s_i is the sign of the i^{th} edge to ensure field continuity between elements , (x_i, y_i) are the global coordinates the local nodes, (z_l, z_u) are the global coordinates of the upper and lower faces of the prism, $c = z_u - z_l$ is the height of the prism, and S^e is the area of the triangle that forms the top (or bottom) of the prism. For the vertical edges, k_1 and k_2 are defined in Table 1

Table 1. Definition of the indices used to construct the vertical prism expansion functions.

χ	k_1	k_2
7	2	3
8	3	1
9	1	2

where χ is the local edge number and (k_1, k_2) indicate local nodes. The curls of these basis functions are defined as

$$\nabla\times\mathbf{V}_i = -\frac{l_i s_i}{2cS^e}[(x-x_i)\hat{\mathbf{x}} + (y-y_i)\hat{\mathbf{y}} - 2(z-z_l)\hat{\mathbf{z}}],$$
$$\nabla\times\mathbf{M}_i = \frac{l_i s_i}{2cS^e}[(x-x_i)\hat{\mathbf{x}} + (y-y_i)\hat{\mathbf{y}} + 2(z_u-z)\hat{\mathbf{z}}],$$
$$\nabla\times\mathbf{K}_i = \frac{[(x_{k2}-x_{k1})\hat{\mathbf{x}} + (y_{k1}-y_{k2})\hat{\mathbf{y}}]}{2S^e}. \tag{8}$$

Note that these expansion functions are functionally identical to [0]; however, since they are expressed in global rather than local coordinates, it is relatively easy to use these functions in conjunction with anisotropic materials specified in terms of global properties.

Right Distorted Hexahedrals

A common example of a regular hexahedra element is the brick element where all the edges are either parallel or orthogonal to any other edge in the element [0]. Distorted hexahedral elements have edges that are not necessarily parallel or orthogonal to the other edges. Distorted hexahedral have been used by [0] and discussed in [0]; however, not in conjunction with other elements. The edges in the extrusion direction are orthogonal to the quadrilateral element used to form the hexahedron. Distorted hexahedral elements are important because they have the ability to model irregular surface geometries with potentially fewer edges than prisms (e.g. narrow slots). This leads to less computational and memory demand for the same geometry modeled with hexahedral elements as opposed to prism elements. Distorted hexahedral elements, however, have the disadvantage of not having closed-form matrix entry formulae and hence require more computational effort as compared to prisms with similar field representation capability.

The basis functions used for hexahedral elements are the so-called rooftop functions. Rooftop basis functions are most often used in brick elements [0-0]. Brick elements are very easy to use but suffer from the fact that they can only model Cartesian-type geometries effectively. In order to model more irregular geometries distorted hexahedral elements can be used. Due to their distortion however the integrals in (5) can be very difficult to compute numerically. Numerical integration over brick shaped volumes is readily

implemented and for this reason it is advantageous if a hexahedral element is mapped into a brick before integration. Figure 3 shows the transformation of a distorted hexahedral element in the (x, y, z) coordinate system to a unit cube in the (ξ, η, ς) coordinate system.

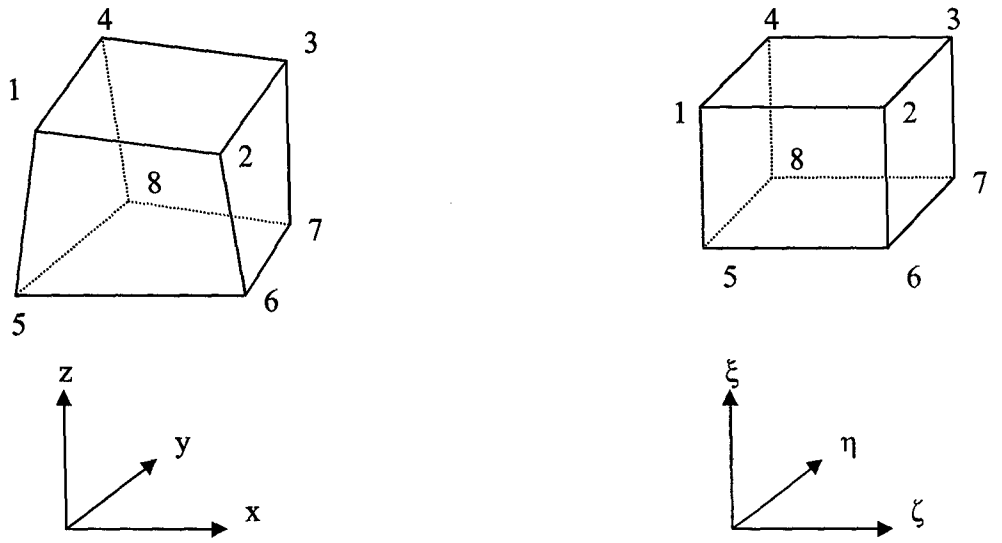

Figure 3: Hexahedral in (x, y, z) coordinates mapped into a cube in (ξ, η, ς) coordinates.

where the edges of the hexahedral and the brick are defined in Table 2.

Table 2 : Local edge numbering for a distorted hexahedral element.

Edge	Node 1	Node2
1	1	2
2	3	4
3	1	4
4	2	3
5	5	6
6	7	8
7	5	8
8	6	7
9	1	5
10	2	6
11	3	7
12	2	6

From [0] the vector edge-based basis functions can be written as

$$\mathbf{N}_i = \frac{l_i s_i}{8}(1 + \eta_i \eta)(1 + \zeta_i \zeta)\nabla \xi \tag{9}$$

for the edges parallel to the ξ direction

$$\mathbf{N}_i = \frac{l_i s_i}{8}(1 + \xi_i \xi)(1 + \zeta_i \zeta)\nabla \eta \tag{10}$$

for the edges parallel to the η direction, and finally

$$\mathbf{N}_i = \frac{l_i s_i}{8}(1 + \xi_i \xi)(1 + \eta_i \eta)\nabla \zeta \tag{11}$$

for the edges parallel to the ζ direction, where l_i denotes the length of the i^{th} edge. Based on the definition of the gradient, these equations can be equivalently written as

$$\begin{aligned}
\mathbf{N}_i &= \frac{l_i s_i}{8}(1+\eta_i\eta)(1+\zeta_i\zeta)\hat{\xi}, \\
\mathbf{N}_i &= \frac{l_i s_i}{8}(1+\xi_i\xi)(1+\zeta_i\zeta)\hat{\eta}, \\
\mathbf{N}_i &= \frac{l_i s_i}{8}(1+\eta_i\eta)(1+\xi_i\xi)\hat{\zeta}.
\end{aligned} \tag{12}$$

Therefore, the basis functions for hexahedral elements are now defined in the mapped coordinate system where numerical integration can be performed over a cube rather than a hexahedral volume.

The integrands in (5) are still represented in terms of global Cartesian coordinates. Defining the Jacobian matrix as

$$\mathbf{J} = \begin{bmatrix} \frac{\partial x}{\partial \xi} & \frac{\partial y}{\partial \xi} & \frac{\partial z}{\partial \xi} \\ \frac{\partial x}{\partial \eta} & \frac{\partial y}{\partial \eta} & \frac{\partial z}{\partial \eta} \\ \frac{\partial x}{\partial \zeta} & \frac{\partial y}{\partial \zeta} & \frac{\partial z}{\partial \zeta} \end{bmatrix} \tag{13}$$

the elemental volume of the integral can be written as [0]

$$dV = dxdydz = \det[\mathbf{J}]d\xi d\eta d\zeta \,. \tag{14}$$

From [0] the following vector operations can be defined

$$\hat{\mathbf{z}} \cdot (\nabla \times \mathbf{N}) = \frac{1}{\det[\mathbf{J}]}\left[\frac{\partial N^{\eta}}{\partial \xi} - \frac{\partial N^{\xi}}{\partial \eta}\right], \tag{15}$$

$$(\nabla \times \mathbf{N}) = \frac{1}{\det[\mathbf{J}]} \times \left[\hat{\xi}\left(\frac{\partial N^{\zeta}}{\partial \eta} - \frac{\partial N^{\eta}}{\partial \zeta}\right) + \hat{\eta}\left(\frac{\partial N^{\xi}}{\partial \zeta} - \frac{\partial N^{\zeta}}{\partial \xi}\right) + \hat{\zeta}\left(\frac{\partial N^{\eta}}{\partial \xi} - \frac{\partial N^{\xi}}{\partial \eta}\right)\right].$$

The above equations can be used to derive the equations needed to implement the FE-BI method using hexahedral elements.

Mixed Element Formulation

Traditional formulations of the FE-BI method use one of the previous two elements described as the sole type of element used to model the geometry. This works well in practice and many implementations of this type have been successful. Each method has its advantages and disadvantages as described previously. To gain benefits not obtainable using one element or the other, the two types of elements can be combined. This allows the use of prism elements where their flexibility is needed, such as at sharp contours and areas of rapid varying fields, while still allowing the use of hexahedral elements where fewer unknowns are needed, such as areas of slowly varying fields or for narrow slots. Only a few additional equations need to be introduced in order to make this mixed element formulation possible. To be more specific, only the boundary integral terms where a prism edge is interacting with a hexahedral edge need to be derived.

The equations for mixed element interactions via the boundary integral can be derived by using the basis functions for the triangular and quadrilateral elements in (5). For the case when triangles are used as test elements and quadrilaterals are used as source elements, the following equations are used

$$I_{ij}^{BI(1)} = \frac{k_0^2}{2\pi}\int_S \int_{-1}^{1}\int_{-1}^{1} [\mathbf{W}_i \cdot (\hat{\mathbf{x}}\hat{\mathbf{x}} + \hat{\mathbf{y}}\hat{\mathbf{y}}) \cdot \mathbf{N}_j] \frac{e^{-jk_0 R}}{R} \det[\mathbf{J}_j] d\xi' d\eta' dS', \tag{17}$$

$$I_{ij}^{BI(2)} = \frac{1}{2\pi}\int_S \int_{-1}^{1}\int_{-1}^{1} \nabla \cdot (\hat{\mathbf{z}} \times \mathbf{W}_i) \nabla' \cdot (\hat{\mathbf{z}} \times \mathbf{N}_j) \frac{e^{-jk_0 R}}{R} \det[\mathbf{J}_j] d\xi' d\eta' dS', \tag{18}$$

where $R = \sqrt{(x-x')^2 + (y-y')^2}$ (16)

Conversely when quadrilaterals are used as test elements and triangles are used as source elements, the following equations are derived.

$$I_{ij}^{BI(1)} = \frac{k_0^2}{2\pi}\int_{-1}^{1}\int_{-1}^{1}\int_{S'} [\mathbf{N}_i \cdot (\hat{\mathbf{x}}\hat{\mathbf{x}} + \hat{\mathbf{y}}\hat{\mathbf{y}}) \cdot \mathbf{W}_j] \frac{e^{-jk_0 R}}{R} \det[\mathbf{J}_i] dS' d\xi d\eta, \tag{19}$$

$$I_{ij}^{BI(2)} = \frac{1}{2\pi}\int_{-1}^{1}\int_{-1}^{1}\int_{S'} \nabla \cdot (\hat{\mathbf{z}} \times \mathbf{N}_i) \nabla' \cdot (\hat{\mathbf{z}} \times \mathbf{W}_j) \frac{e^{-jk_0 R}}{R} \det[\mathbf{J}_i] dS' d\xi d\eta. \tag{20}$$

Using the following relations

$$\nabla \cdot (\hat{\mathbf{z}} \times \mathbf{N}_i) = \frac{l_i s_i}{\det[\mathbf{J}_i]}\left(\frac{\partial N_i^{\xi}}{\partial \eta} - \frac{\partial N_i^{\eta}}{\partial \xi}\right), \tag{21}$$

$$\nabla \cdot (\hat{\mathbf{z}} \times \mathbf{W}_i) = -\frac{l_i s_i}{S_i^e}, \tag{22}$$

the equations needed to implement the mixed element formulation are written

$$\begin{aligned}
{}^{\xi p}I_{ij}^{BI(1)} &= -\frac{k_0^2 l_i l_j s_i s_j}{16\pi S_j^e}\int_{-1}^{1}\int_{-1}^{1}\int_{S'}(1+\eta_i\eta)\left[(x'-x_j)\frac{\partial\xi}{\partial y}-(y'-y_j)\frac{\partial\xi}{\partial x}\right]\frac{e^{-jk_0R}}{R}\det[\mathbf{J}_i]dS'd\xi d\eta,\\
{}^{\eta p}I_{ij}^{BI(1)} &= -\frac{k_0^2 l_i l_j s_i s_j}{16\pi S_j^e}\int_{-1}^{1}\int_{-1}^{1}\int_{S'}(1+\xi_i\xi)\left[(x'-x_j)\frac{\partial\eta}{\partial y}-(y'-y_j)\frac{\partial\eta}{\partial x}\right]\frac{e^{-jk_0R}}{R}\det[\mathbf{J}_i]dS'd\xi d\eta,\\
{}^{p\xi}I_{ij}^{BI(1)} &= -\frac{k_0^2 l_i l_j s_i s_j}{16\pi S_i^e}\int_{S'}\int_{-1}^{1}\int_{-1}^{1}(1+\eta_j\eta)\left[(x-x_i)\frac{\partial\xi'}{\partial y}-(y-y)\frac{\partial\xi'}{\partial x}\right]\frac{e^{-jk_0R}}{R}\det[\mathbf{J}_j]dSd\xi' d\eta',\\
{}^{p\eta}I_{ij}^{BI(1)} &= -\frac{k_0^2 l_i l_j s_i s_j}{16\pi S_i^e}\int_{S'}\int_{-1}^{1}\int_{-1}^{1}(1+\xi_j\xi)\left[(x-x_i)\frac{\partial\eta'}{\partial y}-(y-y)\frac{\partial\eta'}{\partial x}\right]\frac{e^{-jk_0R}}{R}\det[\mathbf{J}_j]dSd\xi' d\eta',
\end{aligned} \tag{23}$$

and

$$\begin{aligned}
{}^{\xi p}I_{ij}^{BI(2)} &= -\frac{l_i l_j s_i s_j \eta_i}{8\pi S_j^e}\int_{-1}^{1}\int_{-1}^{1}\int_{S'}\frac{e^{-jk_0R}}{R}dS'd\xi d\eta,\\
{}^{\eta p}I_{ij}^{BI(2)} &= \frac{l_i l_j s_i s_j \xi_i}{8\pi S_j^e}\int_{-1}^{1}\int_{-1}^{1}\int_{S'}\frac{e^{-jk_0R}}{R}dS'd\xi d\eta,\\
{}^{p\xi}I_{ij}^{BI(2)} &= -\frac{l_i l_j s_i s_j \eta_j}{8\pi S_i^e}\int_{S'}\int_{-1}^{1}\int_{-1}^{1}\frac{e^{-jk_0R}}{R}dSd\xi' d\eta',\\
{}^{p\eta}I_{ij}^{BI(2)} &= \frac{l_i l_j s_i s_j \xi_j}{8\pi S_i^e}\int_{S'}\int_{-1}^{1}\int_{-1}^{1}\frac{e^{-jk_0R}}{R}dSd\xi' d\eta',
\end{aligned} \tag{24}$$

where p denotes the fact the either the test or source edge are associated with a prism element.

III. Numerical Results

To validate this mixed element formulation, two simple test cases were constructed. The first was a 3cm x 2cm slot antenna cut into a 6cm x 5cm x 2cm cavity. The cavity was filled with a dielectric material with a dielectric constant of $\varepsilon_r = 2.17$. The geometry was modeled once with only prism elements and a second time with a mixture of prism elements and hexahedral elements. The RCS of this antenna is shown in Figures 4 and 5.

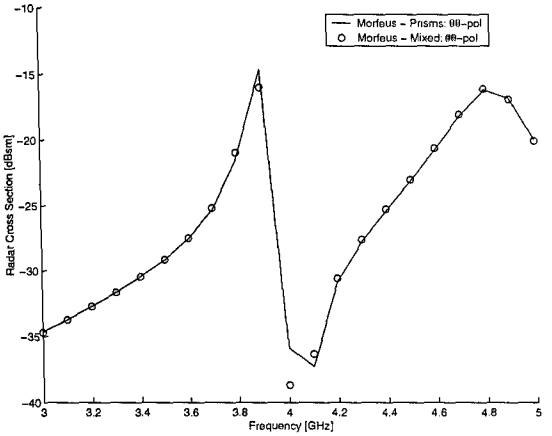

Figure 4: Radar Cross Section of a 6cm x 5cm x 2cm cavity with a 3cm x 2cm slot aperture, θθ-pol.

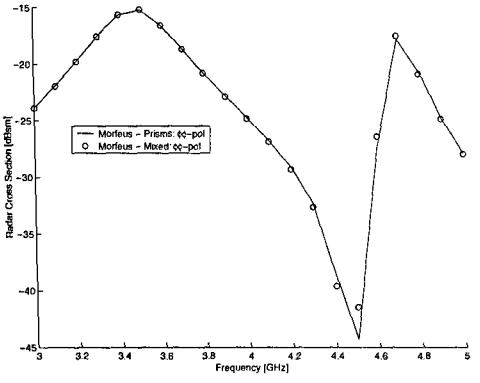

Figure 5: Radar Cross Section of a 6cm x 5cm x 2cm cavity with a 3cm x 2cm slot aperture, φφ-pol.

The results above show that the mixed element formulation is nearly identical to the single element formulation when modeling the radar cross-section of the slot antenna.

The second test case consisted of a 3cm x 2cm patch antenna residing in a 6cm x 4cm x 0.0762cm cavity filled with a dielectric material with $\varepsilon_r = 3.2$. The patch antenna was excited by a probe feed located at x = 3cm, y = 2.1cm. As with the slot antenna this antenna was modeled once with only prisms and again with a mixture of prism elements and hexahedral elements. Figure 6 shows the radiation pattern of the patch antenna at 5.4 GHz and Figure 7 shows the input resistance of the probe feed from 5-6 GHz.

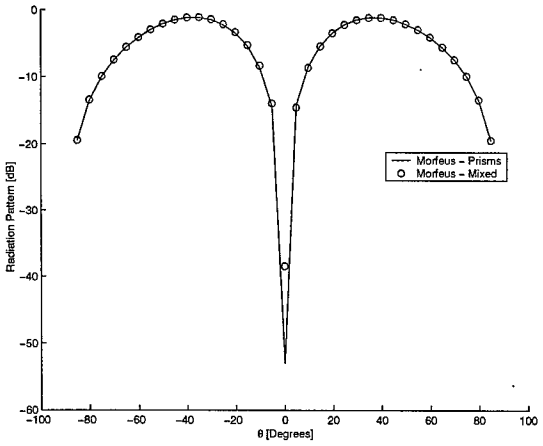

Figure 6: Normalized radiation pattern for a 3cm x 2cm patch antenna in 6cm x 4cm x 0.0762cm cavity.

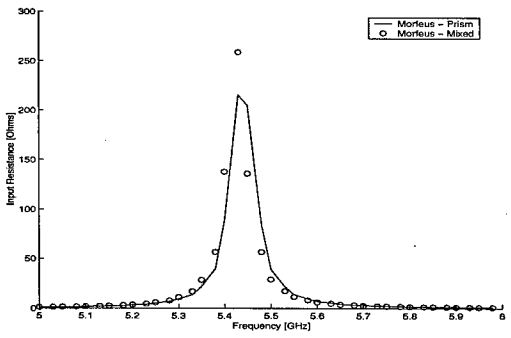

Figure 7: Input resistance of a 3cm x 2cm patch antenna in 6cm x 4cm x 0.0762cm cavity.

The above results show that the mixed element formulation again matches the prism-only formulation results very closely. Different mesh densities around the feed point for the two different methods cause the discrepancy in the value of the input resistance at the resonant point of the patch antenna. Due to the extreme local nature of input impedance small changes in electric field values caused by slightly different sampling rates at the feed point can lead to moderately different results for the value of the input impedance. Also, probe feeds such as the one used in the above example can be extremely sensitive to small changes in the field, which makes them somewhat unreliable for accurate simulations of input impedance value. The most important result in the above example is that the structure has a resonant point at the same frequency using both the prism element formulation and the mixed element formulation.

IV. Solution Efficiency Comparison

To compare and contrast the computational demand required to model geometries with only prism elements as opposed to a mixture of prism and hexahedral elements a few, more complex, cases were considered. These cases were chosen since they represent a class of problems where the triangles used with prisms to represent the aperture, "oversample" the aperture from an electromagnetic viewpoint. This is best understood by considering a narrow slot antenna. Since the electric fields in the slot have only a component perpendicular to the slot sides, quadrilateral elements very efficiently model this slot. In contrast, using an identical sampling density, triangle elements would require one additional degree-of-freedom (e.g. edge) per equivalent quadrilateral element.

The first of these cases included a four-arm spiral antenna with one, two, and three turns. The second was an I-dipole array consisting of one, four, nine, and sixteen dipoles. The time required computing a single radiation pattern

cut, with an INTEL XEON 550 MHz processor running the Linux operating system, was recorded for each of the aforementioned geometries. Figure 8 shows examples of the different geometries used for the results along with the meshing used. Table 3 describes the different mesh parameters for the example geometries. A single pattern cut was computed in the X-Z plane at a frequency of 12 GHz for the spiral antenna and 4GHz for the I-dipole array. Figure 9 illustrates the time required to compute a radiation pattern cut for the four-arm spiral antenna versus the number of turns in the spiral. Figure 10 illustrates the time required to compute a single radiation pattern cut for the I-dipole array versus the number of dipoles in the array.

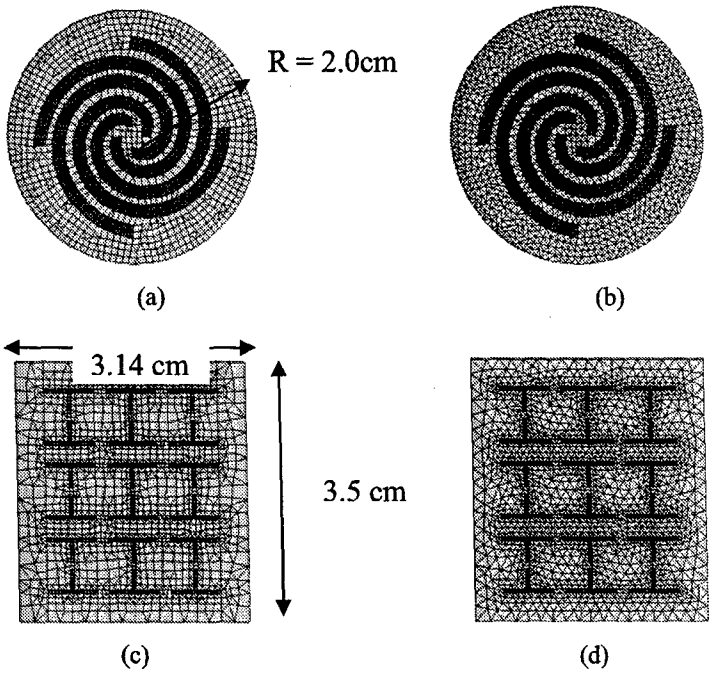

Figure 8: A four-arm, one-turn spiral and a 3x3 I-Dipole array (a) spiral with mixed elements, (b) spiral with prism elements, (c) I-Dipole array with mixed elements, (d) I-Dipole with prism elements.

Table 3: Mesh comparison for a four-arm, one-turn spiral antenna and a 3x3 I-Dipole array.

	Spiral Mixed	Spiral Prism	I-Dipole Mixed	I-Dipole Prism
Surface Elements	1313	2338	2280	3600
Surface Edges	2544	3569	3980	5437
Surface Unknowns	**1296**	**1941**	**2880**	**4013**
Total Elements	14443	25718	15960	25200
Total Edges	44080	56380	43747	56362
Total Unknowns	**37684**	**48579**	**37705**	**48539**

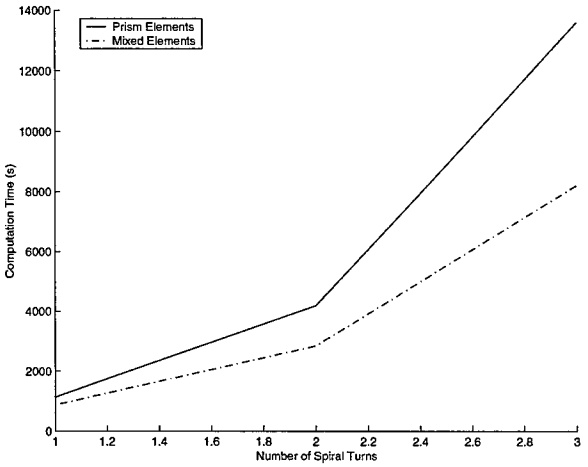

Figure 9: Required computation time for a single radiation pattern cut for a four arm spiral antenna.

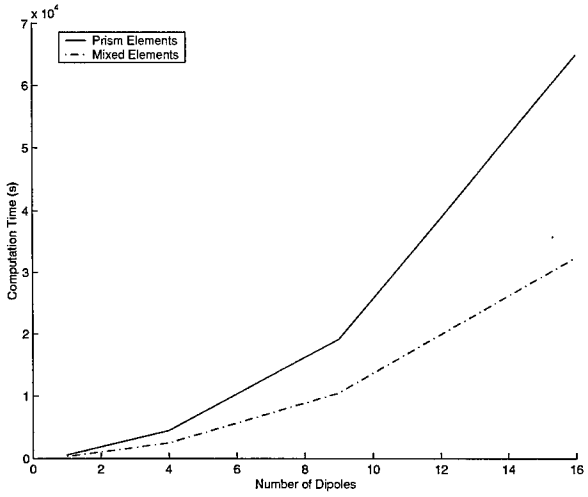

Figure 10: Required computation time for a single radiation pattern cut for an I-dipole array antenna.

As can be seen from the above results the mixed element formulation scales much better for geometrically constrained problems, such as spiral antennas and I-dipole arrays, as compared to the prism-only formulation.

V. Conclusions

A mixed element formulation was developed to model three-dimensional planar cavity-backed aperture antennas. This formulation was shown to be equivalent to a formulation using only prism elements but was more efficient in terms of memory and computational demand. The main memory and computational savings were due to the fact that the mixed element formulation produced fewer surface unknowns, for a comparable electromagnetic representation, than the prism element formulation for the same geometry.

Slight discrepancies between the mixed element and prism element formulations were seen in the modeling of impedance for complex geometries. Dissimilar mesh densities surrounding the feed points causing different input powers to be produced at the feeds caused these discrepancies. These discrepancies were not seen in radar cross-section simulations as RCS measurements do not include a feed model.

REFERENCES

[1] H. Nakano, K. Hirose, I. Ohshima, and J. Yamauchi, "An integral equation and its application to spiral antennas on semi-infinite dielectric materials," *IEEE Transactions on Antennas and Propagation*, 47, p. 267-274, Feb. 1998.

[2] W.C. Chew, J.M. Jin, E. Michielssen, and J.M. Song, Fast and Efficient Algorithms in Computational Electromagnetics, Artech House, 2001.

[3] J.L. Volakis, A. Chatterjee, L.C. Kempel. Finite Element Method for Electromagnetics. IEEE Press, New York, 1998.

[4] J.M. Jin. The Finite Element Method in Electromagnetics. John Wiley and Sons Inc, 1993.

[5] J. Gong, J.L. Volakis, A. Woo, and H.T. Wang, "A hybrid finite element-boundary integral method for the analysis of cavity-backed antennas of arbitrary shape," *IEEE Transactions on Antennas and Propagation*, 42, p. 1233-1242, Sept. 1994.

[6] L.C. Kempel and J.L. Volakis, "Scattering by cavity-backed antennas on a circular cylinder," *IEEE Trans.*

Antennas Propagation., 42, pp. 1268-1279, Sept. 1994.

[7] L.C. Kempel, J.L. Volakis, and R.J. Sliva, "Radiation by cavity-backed antennas on circular cylinder," *IEE Proc.-Microw. Antennas Propag.*, 142, pp. 233-239, June 1995.

[8] X-Q Sheng, J-M Jin, J. Song, C-C Lu, and W.C. Chew, "On the formulation of hybrid finite-element and boundary-integral methods for 3-D scattering," *IEEE Transactions on Antennas and Propagation*, 46, p. 303-311, March. 1998.

[9] C.A. Macon, L.C. Kempel, and S.W. Schneider, "Radiation and Scattering by Complex Conformal Antennas on a Circular Cylinder," *Adv. Comp. Math.*, 16, pp. 191-209, 2002.

[10] F. Bilotti, A. Toscano, and L. Vegni, "FEM-BEM formulation for the analysis of cavity-backed patch antennas on chiral substrates," *IEEE Transactions on Antennas and Propagations*, 51, pp. 1829-1836, August 2003.

[11] C-W Wu, L.C. Kempel, and E.J. Rothwell, "Hybrid Finite Element-Boundary Integral Method for Cavities Recessed in an Elliptic Cylinder," *IEEE Transactions on Antennas and Propagations*, 51, pp. 306-311, Feb. 2003.

[12] C.A. Macon, L.C. Kempel, S.W. Schneider, and K.D. Trott, "Modeling Conformal Antennas on Metallic Prolate Spheroid Surfaces Using a Hybrid Finite Element Method," *IEEE Transactions on Antennas and Propagations*, 52, pp. 750-758, March 2004.

[13] K.K. Mei, "Unimoment method of solving antenna and scattering problems," *IEEE Transactions on Antennas and Propagations*, 22, p. 760-766, Nov. 1974.

[14] J. Liu and J.M. Jin, "A novel hybridization of higher order finite element and boundary integral methods for electromagnetic scattering and radiation problems, *IEEE Transactions on Antennas and Propagations*, 49, p. 1794-1806, Dec. 2001.

[15] G.E. Antilla, Radiation and Scattering from Complex Three-Dimensional Geometries using a Curvilinear Hybrid Finite Element-Integral Equation Approach, Ph.D. Dissertation, University of California at Los Angeles, 1993.

[16] L.C. Kempel, "Implementation of Various Hybrid Finite Element-Boundary Integral Methods: Bricks, Prisms, and Tets," 1999 ACES Meeting, Monterey, CA, pp. 242-249, 1999.

[17] C-T Tai, Dyadic Green Functions in Electromagnetic Theory, 2nd ed., Piscataway, NJ: IEEE Press, 1994.

[18] A.F. Peterson, S.L. Ray, R.Mittra. Computational Methods for Electromagnetics. IEEE Press, New York, 1998.

[19] S.M. Rao, D.R. Wilton, A.W. Glisson. "Electromagnetic Scattering by Surfaces of Arbitrary Shape", *IEEE Transactions on Antennas and Propagations*, 30, pp. 409-418, May 1982.

[20] T. Ozdemir and J.L. Volakis, "Triangular prisms for edge-based vector finite element analysis of conformal antennas *IEEE Transactions on Antennas and Propagations*, 45, p. 788-797, May 1997.